Flow-Substrate Interactions in Aggrading and Degrading Submarine Channels

Anjali M. Fernandes[1,2], Jim Buttles[1], David Mohrig[1], Kyle M. Straub[3]

[1]*The Center for Integrative Geoscience, University of Connecticut, Storrs, Connecticut, USA.*

[2]*The Jackson School of Geosciences, The University of Texas at Austin, Texas, USA.*

[3]*Department of Earth and Environmental Sciences, Tulane University, 6823 St. Charles Avenue, New Orleans, Louisiana 70118-5698, USA*

Email: anjali.fernandes@uconn.edu

Keywords: Turbidity currents; submarine channels; submarine canyons; boundary layer roughness; flow-separation zones; erosional bedforms; detachment-limited channels; transport-limited channels; Shields scaling

ABSTRACT

Connecting real time measurements of current-bed interactions to the temporal evolution of submarine channels can be extremely challenging in natural settings. We present a suite of physical experiments that offer insight into the spectrum of interactions between turbidity currents and their channels, from (i) detachment-limited erosion to (ii) transport-limited erosion to (iii) pure deposition. In all three cases channel sinuosity influenced patterns of erosion and deposition; the outsides of bends displayed the highest erosion rates in the first two cases, whereas the outsides of bends were associated with the highest deposition rates the third. We connect the evolution of these channels to the turbulence of the near-bed boundary layer. In the erosional experiments both channel beds roughened through time, developing erosional bedforms or trains of ripples. Reynolds estimates of boundary layer roughness indicate that, in both erosional cases, the near-bed boundary layer roughened from smooth or transitionally rough to rough, whereas the depositional channel appears to have remained consistently smooth. Our results suggest that, in the absence of any changes from upstream, erosion in submarine

channels erosion is a self-reinforcing mechanism whereby developing bed roughness increases turbulence at the boundary layer, thereby inhibiting deposition, promoting sediment entrainment and enhancing channel relief; deposition occurs in submarine channels when the boundary layer remains smooth, promoting aggradation and loss of channel relief.

INTRODUCTION

Continental margins are patterned with channels and canyons that convey large volumes of sediment to the deep ocean. These channels evolve through erosion and/or deposition, often aggrading over significant vertical distances (Pirmez et al., 2000), or by carving canyons (Babonneau et al., 2010; Conway et al., 2012) many hundreds of meters deep. Physical experiments can offer insight into current-bed interactions. Such measurements are challenging to acquire in natural settings and even more challenging to relate to the temporal evolution of submarine channels (Khripounoff et al., 2003; Xu et al., 2004, 2013; Xu, 2010; Hughes Clarke, 2016; Symons et al., 2017; Azpiroz-Zabala et al., 2017b, 2017a). In the past, some experiments e.g. (Mohrig and Buttles, 2007; Straub et al., 2008; Janocko et al., 2013) focused on purely depositional turbidity currents that were suspension-dominated, whereas others investigated erosional currents that modified channels primarily through bedload-transport (Métivier et al., 2005; Amos et al., 2010). Here we present three experiments which we use to explore the processes that shape submarine channels, along the continuum of intensely erosional to purely depositional in connection to the hydraulic characteristics of the near-bed boundary layer, across this spectrum of behaviour.

Detachment-limited and transport-limited erosion in terrestrial landscapes

Terrestrial channels eroding into bedrock have been modeled using: a) a detachment-limited model in which the resistance of the substrate is the limiting factor that controls the erosion rate, and b) a transport-limited model where the erosion rate is limited by the ability to transport the eroded sediment (Howard, 1980, 1994; Whipple, 2004). Detachment-limited erosion is more sensitive to local conditions (e.g. topographic or bed roughness) rather than reach-averaged conditions (e.g. discharge; (Johnson and

Whipple, 2007). Erosion generally takes place through abrasion and wear by the impacts of sediment being transported by the flow, and turbulence generated by evolving bed roughness. These channels are characterized by knickpoints, inner channels, scour holes, grooves, and sculpted bedforms (Whipple, 2004). The transporting currents are efficient at removing sediment in transport from upstream and at entraining material from the local substrate.

When the removal of eroded sediment is not efficient, sediment is stored in patches on the bed, protecting the bed from further erosion in a phenomenon referred to as the 'cover-effect' (Johnson et al., 2009). Erosional channels with abundant sediment cover on the channel bed are referred to as "transport-limited" (Shepherd and Schumm, 1974; Sklar and Dietrich, 2004; Whipple, 2004; Johnson and Whipple, 2007). Partially-alluviated erosional channels scouring into compact, indurated sediment have been observed in depositional landscapes such as the Mississippi River Delta (Edmonds et al., 2011; Nittrouer et al., 2011a), where cover effects are particularly evident. Channel bottoms display deep scours where they are devoid of alluvial cover at the outsides of river bends. All natural erosional channels can be expected to display some combination of detachment-limited and transport-limited behaviour (Whipple, 2004). Here we use 2 experiments to study the characteristics of detachment-limited and transport-limited erosion in submarine channels. For completeness, we incorporate data from an aggradational channel experiment (Straub et al., 2008). We use these experiments to explore the role of the near-bed boundary layer in the spectrum of forms and deposit characteristics observed.

<u>Dynamic scaling of experiments to natural systems</u>

Laboratory experiments have historically been compared to natural systems by using three dimensionless variables: (1) the densimetric Froude number (Fr_d), (2) the Reynolds number (Re), and (3) the ratio of current shear velocity u^* to particle fall velocity w_s (Middleton, 1966; Baas et al., 2004; Yu et al., 2006; Mohrig and Buttles, 2007; Straub et al., 2008; Amos et al., 2010; Rowland et al., 2010; Cantelli et al., 2011). The first parameter, the Froude number, defines the ratio between momentum and gravitational forces within the transporting current and is traditionally maintained equal or similar to natural analogues. The Reynolds number, which quantifies the turbulence of the currents, cannot be equal to natural flows in scaled-down laboratory settings. The third parameter, also referred to as a Shield's parameter (Shields, 1936; Bagnold, 1966; Smith and Hopkins, 1971; van Rijn Leo C., 1984; Nino et al., 2003), characterizes how sediment is transported. Flows in which the turbulent shear, expressed as the shear velocity u*, is significantly larger than the gravitational settling velocity w_s will be more competent at transporting sediment in suspension over significant distances (Shields, 1936; Smith and Hopkins, 1971) and will prelude sediment-bed interactions over short length scales; if u* is comparable to w_s, sediment can be transported as either saltating or incipiently suspended load, dependent upon the intensity of turbulence associated with current-bed interactions. In channelized turbidity currents, the intensity of near-bed turbulence is the combined result of turbulent eddies shed at the scale of individual particles (de Leeuw et al., 2016), of bed roughness (e.g. bedforms, scours, etc.) (Eggenhuisen et al., 2010; Eggenhuisen and McCaffrey, 2012; Arfaie et al., 2018), as well as of planform irregularities (e.g. curved channels) (Straub et al., 2011) which can impart turbulent shear from non-uniform spatial accelerations. The magnitude of turbulence will scale with the magnitudes of fluid shear (u*) and the size of the element under consideration (e.g. particle diameter, dune height, scour depth, bend amplitude, etc.). Turbulence associated with these roughness scales contributes to entrainment of sediment from the bed and walls of channels, and encourages vertical mixing which maintains sediment in suspension. The ratio between fluid shear and the viscous forces which act to damp turbulence can be used to characterize the roughness of the near-bed boundary layer (Garcia, 2008).

De Leeuw et al. (2016) argued that realistic turbulence-sediment interactions were critical for effectively modelling submarine channel inception and evolution, and proposed a scaling approach defined by the ratio of the Shield's parameter to the particle Reynolds number (Re_p). In this scaling approach, the Shield's parameter is held similar between experimental and naturally occurring density currents, but the similarity between the particle Reynolds numbers is relaxed as long as the boundary layer is rough or transitionally rough (Garcia, 2008; de Leeuw et al., 2016). Leeuw et al. (2017) noted that density currents in most previous experiments were highly depositional because the boundary layers were hydraulically smooth and/or the Shields parameter fell below the initiation of suspension.

In Figure 1, we adopt the Shield's scaling proposed by de Leeuw et al. (2016) to compare flow and sediment transport characteristics of the three experiments presented here to past experimental and field measurements. Although the shear stresses associated with all three experiments exceeded the threshold for the initiation of suspension, they straddle the threshold between hydraulically smooth and transitionally rough boundary layers. Furthermore, Experiments 1 and 2 scale best with recent field observations of flow and transport in natural systems. Using sediment with much lower densities than silica in these experiments allowed us to use sand-sized particles that had transitionally rough boundary layers and high Shields parameters, and were therefore easy to suspend and maintain in suspension.

Experiment Design

In each experiment, calcium chloride salt and water (and sediment, when it was used), were mixed together in a reservoir, until the salt was completely dissolved. The mixture was agitated over several hours and allowed to cool to room temperature, as the dissolution of this salt in water is an exothermic process. Once at room temperature, the mixture was pumped up to a constant head tank and then allowed to flow into the experimental basin at a controlled rate set by the constant hydraulic head and a system of valves. The two experimental basins were designed along similar lines, shown by the generalized schematic in Figure 2. In all experiments, density currents were released into an experimental channel through a box with two perforated screens designed to extract momentum from flows. The pre-formed channels were built upon a platform separated from the walls of the basin by deep moats that prevented currents from reflecting off the basin walls. Saline fluid was not allowed to collect in the basin and was extracted through the floor drains as it flowed off the raised platform. The water level in the basin was maintained with a constant flux of fresh water and overflow drainage through a weir. The basin used in Experiment 1 was 8 m long, 6 m wide and 2 m deep. The basin used for Experiments 2 & 3 was 5 m long, 4.5 m wide and 0.8 m deep. In all experiments, the channel was constructed diagonally across the false floor.

The channels used in these experiments were designed with similar sinuosity, but different sediment and flow properties (Table 1). In Experiment 1, the channel was built entirely out of a weakly cohesive mixture of acrylic particles (specific gravity = 1.15) and clay positioned on top of a sloping ramp. The sediment was mixed in a 10:1 volumetric ratio. The first two currents released into the channel were saline density currents (excess density = 4%). These were followed by three more density currents that carried a 2% volumetric concentration of suspended acrylic sediment.

In Experiment 2 a saline density current (excess density = 3.32%) was released through the experimental channel which consisted of a cohesionless, 2-cm thick bed of acrylic particles draped over a sinuous channel form built from concrete. In Experiment 3 sixteen purely depositional currents flowed through a channel constructed of concrete with a thin layer of silica sediment on the bed. Currents had an excess density of 2.1%. 33% of this excess density was supplied by suspended sediment in the current, and the remaining 67% was from dissolved salt. High-resolution bathymetry maps (horizontal resolution = 4mm; vertical resolution ~100 microns for Experiments 1 & 2; ~1mm for Experiment 3), collected before and after each flow defined patterns of bed change for all three cases. Key geometric and dynamic properties of the experimental designs are compiled in Table 1.

Table 1: Summary of geometric and dynamic properties of Experiments 1, 2 and 3.

	Parameter	Experiment 1	Experiment 2	Experiment 3
Channel geometry	Channel depth (m)	0.15	0.09	0.11
	Channel width (m)	0.50	0.40	0.40
	Down-channel slopes (degrees)	7.00	2.00	1.00
	Initial mean thickness of erodible bed (m)	0.07	0.02	0.00
	Channel sinuosity	1.15	1.28	1.28
Sediment properties	Sediment density (ρ_s) (kg/m^3)	1150.00	1150.00	2650.00
	D_{1}	49	49	1.7
	D_{10}	88	88	12.9
	D_{25}	127	127	23
	D_{50}	146	146	31
	D_{75}	205	205	41
	D_{90}	243	243	52.1
	D_{99}	340	340	80
Flow properties	Flow thickness (m)	0.10	0.09	0.10
	Current density (ρ_f) (kg/m^3)	1040	1033.20	1021
	Depth-averaged downstream velocity (u) (m/s)	0.10	0.05	0.08
	Shear velocity (u*) (m/s)	0.04	0.03	0.04
	Froude number (Fr)	0.50	0.26	0.56
	Reynolds number (Re)	10000.00	4050.00	8000.00

	Particle Reynolds number (Re_p)	6.53	4.38	1.24
	Shields parameter	13.20	5.56	3.30
	Bed roughness scale (H_{bed}) (m)	0.01 - 0.05	0.01 - 0.02	-
	Reynolds number from bed roughness (Re_{bed})	~650 - 2236	~330- 660	-

Results

Integrating surface change for each flow in all three cases reveal net erosion in Experiments 1 and 2, and net deposition in Experiment 3.

Experiment 1

In Experiment 1, all 5 currents released through the channel modified it through net erosion (Fig. 3 A, Fig. 4). The weakly cohesive bed consisted of sediment that was easily suspended once it detached from the surface (Fig. 1). Extreme run-up of currents onto the outer walls of channel bends occurred, resulting in the formation of a low-velocity flow-separation zone (depth-averaged velocity ~= 1-2 m/s) at the inner bank (Fig. 4G; Fig.5) (Leeder and Bridges, 1975; Fernandes et al., 2018). Erosion occurred beneath the pathway of the high-velocity (depth-averaged velocity = 10m/s) core of the current, which travelled along the outside of bends and created a series of discontinuous scours. Initially, while the channel bed was smooth, the most intense scouring occurred at the outside of bends (Fig. 4A, B, H; Fig. 6). Subsequently, the rough edges of scours became sites of focussed erosion (Fig. 4C-F, I-L; Fig. 6A-C) and resultant elongation of scours resulted in the formation of a discontinuous inner channel (Fig. 7A- B). Focussed erosion at the downstream edges of scours released clouds of suspended sediment that were transported downstream and out of the system. Consecutive inner bank areas were separated by a swath of erosion, and evolved into raised terraces within the low-velocity flow separation zone (Fig. 3A, Fig. 4; (Fernandes et al., 2018). The channel bed evolved from smooth to ornamented, displaying erosional bedforms with centimeter-scale relief (Fig. 3A; Fig. 6). These bed morphologies are similar to those observed in detachment-limited terrestrial channels, where erosion is limited by the strength of the substrate and bed erosion occurs primarily through wear by abrasion and plucking (Whipple et al., 2000; Whipple, 2004). The channel remained net-erosional through its entire length (Fig. 3A; Fig. 4).

Experiment 2

This channel was modified through net-erosion, with a fraction of mobilized sediment leaving the system in suspension while the remainder was reworked into a continuous train of bedforms (Fig. 3B). As in Experiment 1, the high velocity core of the density current travelled along the outsides of bends, resulting in: 1) erosion of sediment at the outer bank, where sediment removal exposed the underlying erosion-resistant channel form in the troughs between sediment-starved bedforms, and 2) deposition at the inner bank, which resulted from the convergence of downstream and cross-stream bedload transport (Fig. 3B, Fig 7C-D). These zones of deposition began just upstream from the points of maximum channel curvature, and were connected across inflection points through the continuous bedform field (Fig. 4B). Erosion in this experiment was less efficient than in Experiment 1. Abundant sediment cover on the channel bed is suggestive of erosional mechanics similar to that of transport-limited erosional terrestrial channels, which are also characterized by alluviated channel beds interrupted by variable degrees of local scouring (Whipple, 2004; Nittrouer et al., 2011a, 2011b), and in which the erosion rate is limited by the ability of the flow to transport the eroded sediment.

Experiment 3

Currents modified this channel via net sediment deposition (Straub et al., 2008). The thickest deposition closely tracked the pathway of the high velocity core, which was inferred to be the pathway of the highest suspended sediment concentration (Fig. 9 of Straub et al., 2008). This resulted in thicker deposits at the outer banks of bends and thinner deposits in low-velocity zones at the inner banks of bends (Fig. 3C, Fig. 7E-F). Deposits from each current draped the entire channel (Fig. 7E-F), and thinned in the downstream direction (Fig. 6D-F). Sediment was primarily transported as and deposited from suspended load. Suspended sediment flux was estimated to be roughly 40 times that of bedload flux (Straub et al., 2008).

Discussion

Boundary layer roughness in erosional and depositional channels

The transporting currents in all three experiments had shear stresses that were high enough to transport sediment in suspension. Yet their temporal evolution spanned the spectrum from intense erosion to pure deposition. In all three cases, planform irregularity influenced the spatial variability in sedimentation and/or erosion by influencing the path of the highest velocities and sediment concentrations. A key difference between the 3 experiments lies in the characteristics of the hydraulic boundary layer and the temporal evolution of the three channels suggests strong agreement with the Shield-scaling predictions of de Leeuw et al., 2016. Particle-scale Reynolds estimates of boundary layer turbulence place Experiment 1 in the transitionally rough hydraulic regime, whereas Experiment 2 was at the approximate boundary between the smooth and transitionally rough regime, and Experiment 3 was squarely within the hydraulically smooth regime. Furthermore, Experiment 1 evolved from a smooth bed to one patterned by scours, grooves and other centimeter-scale erosional bedforms; Experiment 2 evolved from a smooth bed into a semi continuous bedform field. In both erosional experiments the roughening of the channel bed is likely to have encouraged greater turbulence at the near-bed boundary (Fig. 2).

At the start of Experiment 1, the smooth sediment bed was modified by erosion along the pathway of the high velocity core; the magnitude of erosion appeared to be greatest near the outsides of bends (Fig. 4A, B, G, H). Particle Reynolds numbers calculated from mean, depth-averaged downstream velocities at the outsides (0.1 m/s) and insides (0.01 - 0.02 m/s) of bends point to a hydraulically smooth boundary layer within the flow separation zone at the inside of the bend, and a transitionally rough boundary layer at the outside (Fig. 2). The emergence of erosional roughness with 1-5 centimeter relief is likely to have further roughened the boundary layer, prohibiting sediment deposition and increasing erosion at sites with enhanced roughness (Fig. 3A; Fig. 4; Fig.6). Near bed turbulence increased by at least two orders of magnitude (Re_{bed} ~450 for 1cm relief; Re_{bed} ~ 2200 for 5cm relief; Fig. 2), causing a regime shift towards a hydraulically rough boundary layer (Garcia, 2008). Hydraulically smooth boundary layers in flow separation zones at the inner banks (Fig. 2) precluded erosion and very low suspended sediment fluxes were unfavourable for deposition. Overall, Experiment 1 evolved in such a way that sediment entrainment and removal remained efficient through time, and channel relief consistently increased as currents scoured into the ~7cm thick erodible sediment bed (Fig. 6A; Fig 7A). Detachment-limited erosion is indicated by evolution of sculpted erosional bedforms, efficient sediment removal and enhanced erosion linked to local bed roughness. The temporal evolution of this channel therefore offers significant insights into the evolution of topography and flow-bed interactions in detachment-limited erosional submarine channels and canyons e.g. (Conway et al., 2012; Vachtman et al., 2013; Mitchell, 2014) that incise into compacted or indurated fine-grained sediment on the upper continental slope and are efficient, dominantly-erosional conduits for sediment transport into the deep ocean.

Like Experiment 1, Experiment 2 also evolved from a smooth bed to a rough one and the outer banks of bends were sites of enhanced erosion. Using ripple crest height of 1-2 cm as the relevant length scale, Reynolds estimates indicate that the boundary layer evolved to become hydraulically rough (Fig. 2; (Garcia, 2008), though it was at the threshold between hydraulically smooth and transitionally rough at the start of the experiment (Table 1). The Shields parameter for all particle sizes present falls above the threshold for initiation of suspension (Shields, 1936; Bagnold, 1966; Smith and Hopkins, 1971; van Rijn Leo C., 1984; Nino et al., 2003), suggesting that the rate of erosion was limited by the currents' capacity to transport the sediment in suspension, and that the sediment that could not be suspended was transported as bedload. The development of a bedform field, while it likely facilitated sediment entrainment by roughening the boundary layer probably also reduced fluid momentum and the capacity of the current to suspend sediment. This style of transport-limited erosion (Whipple, 2004; Johnson and Whipple, 2007) likely offers insight into the delicate balance of flow-sediment feed-backs that control spatially variable sedimentation and erosion in dominantly bypassing submarine channels on the middle or lower continental slope.

Unlike Experiments 1 and 2, Experiment 3 remained depositional for the duration of the experiment. Straub et al., (2008) noted that super-critically climbing ripples were present over only approximately 5% of the sediment bed. Consistent deposition and reduction in channel relief (Straub et al., 2008) through time suggests that the boundary layer characteristics likely shifted further into the hydraulically smooth regime. We suggest that this style of evolution would be most characteristic of channels near the terminus of submarine transport systems, on terminal lobes on the basin flow where sediment is delivered by depletive flows that are unable to re-entrain sediment.

CONCLUSIONS

It is extremely challenging to connect current-bed interactions to the temporal evolution of submarine channels in natural settings (Khripounoff et al., 2003; Xu et al., 2004, 2013; Xu, 2010; Hughes Clarke, 2016; Symons et al., 2017; Azpiroz-Zabala et al., 2017b, 2017a). We used 3 experiments in which we relate near bed turbulence, as a function of evolving bed roughness, to patterns of erosion and deposition. In all three experiments presented here, channel sinuosity influenced patterns of erosion and deposition. Although the currents used in all three case displayed shear stresses high enough to suspended sediment, the temporal evolution in the turbulence near-bed boundary layer was also very important in deciding whether the channel evolved through erosion or deposition. In the experiments where the boundary layer was transitionally rough the channel evolved through erosion, developing a roughened bed. In both cases, the near-bed boundary layer roughened from smooth or transitionally rough to rough, enhancing near-bed turbulence. When the channel substrate was cohesive, the channel bed evolved through detachment-limited erosion and most of the sediment left the system in suspension. The channel bed was patterned by erosional bedforms, grooves, inner-bank terraces and a semi-continuous inner channels. When the sediment was non-cohesive, the erosion was limited by the ability of the currents to transport sediment and the channel bed evolved into trains of ripples. In contrast, the channel with a hydraulically smooth boundary layer evolved through consistent deposition and the boundary layer appears to have remained hydraulically smooth. To our knowledge, this work presents the first instance in which detachment-limited erosional channels with realistic sediment transport patterns and sediment-turbulence interactions have been designed successfully in laboratory settings. Our results suggest that erosion in submarine channels is a self-reinforcing mechanism whereby developing bed roughness increases turbulence at the boundary layer, enhancing erosion and inhibiting deposition; deposition in submarine channels occurs if the boundary layer is smooth, promoting channel aggradation and loss of channel relief.

Acknowledgements

We thank the Jackson School of Geosciences, the CSM-UT RioMAR Industry Consortium, and Shell International Exploration and Production Inc. for facilities and financial support of this work.

References cited

Alexander, J., McLelland, S.J., Gray, T.E., Vincent, C.E., Leeder, M.R., and Ellett, S., 2007, Laboratory sustained turbidity currents form elongate ridges at channel mouths: Channel mouth deposition from sustained turbidity currents: Sedimentology, v. 55, p. 845–868, doi:10.1111/j.1365-3091.2007.00923.x.

Amos, K.J., Peakall, J., Bradbury, P.W., Roberts, M., Keevil, G., and Gupta, S., 2010, The influence of bend amplitude and planform morphology on flow and sedimentation in submarine channels: Marine and Petroleum Geology, v. 27, p. 1431–1447, doi:10.1016/j.marpetgeo.2010.05.004.

Arfaie, A., Burns, A.D., Dorrell, R.M., Ingham, D.B., Eggenhuisen, J.T., and McCaffrey, W.D., 2018, Optimisation of flow resistance and turbulent mixing over bed forms: Environmental Modelling & Software, v. 107, p. 141–147, doi:10.1016/j.envsoft.2018.06.002.

Azpiroz-Zabala, M., Cartigny, M.J.B., Sumner, E.J., Clare, M.A., Talling, P.J., Parsons, D.R., and Cooper, C., 2017a, A General Model for the Helical Structure of Geophysical Flows in Channel Bends: General model for helical flows in bends: Geophysical research letters, v. 44, p. 11,932–11,941, doi:10.1002/2017GL075721.

Azpiroz-Zabala, M., Cartigny, M.J.B., Talling, P.J., Parsons, D.R., Sumner, E.J., Clare, M.A., Simmons, S.M., Cooper, C., and Pope, E.L., 2017b, Newly recognized turbidity current structure can explain prolonged flushing of submarine canyons: Science advances, v. 3, p. e1700200, doi:10.1126/sciadv.1700200.

Baas, J.H., Van Kesteren, W., and Postma, G., 2004, Deposits of depletive high-density turbidity currents: a flume analogue of bed geometry, structure and texture: Sedimentology, v. 51, p. 1053–1088, doi:10.1111/j.1365-3091.2004.00660.x.

Babonneau, N., Savoye, B., Cremer, M., and Bez, M., 2010, Sedimentary Architecture in Meanders of a Submarine Channel: Detailed Study of the Present Congo Turbidite Channel (Zaiango Project): Journal of Sedimentary Research, v. 80, p. 852–866, doi:10.2110/jsr.2010.078.

Bagnold, R.A., 1966, An Approach to the Sediment Transport Problem from General Physics: U.S. Government Printing Office

Cantelli, A., Pirmez, C., Johnson, S., and Parker, G., 2011, Morphodynamic and Stratigraphic Evolution of Self-Channelized Subaqueous Fans Emplaced by Turbidity Currents: Journal of Sedimentary Research, v. 81, p. 233–247, doi:10.2110/jsr.2011.20.

Cartigny, M.J.B., Eggenhuisen, J.T., Hansen, E.W.M., and Postma, G., 2013, Concentration-dependent flow stratification in experimental high-density turbidity currents and their relevance to turbidite facies models: Journal of Sedimentary Research, v. 83, p. 1047–1065

Conway, K.W., Barrie, J.V., Picard, K., and Bornhold, B.D., 2012, Submarine channel evolution: active channels in fjords, British Columbia, Canada: Geo-Marine Letters, v. 32, p. 301–312, doi:10.1007/s00367-012-0280-4.

Edmonds, D.A., Shaw, J.B., and Mohrig, D., 2011, Topset-dominated deltas: A new model for river delta stratigraphy: Geology.

Eggenhuisen, J.T., and McCaffrey, W.D., 2012, The vertical turbulence structure of experimental turbidity currents encountering basal obstructions: implications for vertical suspended sediment distribution in non-equilibrium currents: Sedimentology, v. 59, p. 1101–1120, doi:10.1111/j.1365-3091.2011.01297.x.

Eggenhuisen, J.T., McCaffrey, W.D., Haughton, P.D.W., and Butler, R.W.H., 2010, Small-Scale Spatial Variability in Turbidity-Current Flow Controlled by Roughness Resulting from Substrate Erosion: Field Evidence for a Feedback Mechanism: Journal of Sedimentary Research, v. 80, p. 129–136, doi:10.2110/jsr.2010.014.

Fernandes, A.M., Mohrig, D., and Buttles, J., 2018, A New Mechanism for Terrace Formation in Submarine Canyons: EarthArXiv. September, v. 1, doi: 10.31223/osf.io/a6p7y

Garcia, M.H., 2008, Sedimentation Engineering: Theories, Measurements, Modeling and Practice: Processes, Management, Modeling, and Practice (Asce Manual and Reports on Engineering Practice No: American Society of Civil Engineers.

Garcia, M., and Parker, G., 1989, Experiments on hydraulic jumps in turbidity currents near a canyon-fan transition: Science, v. 245, p. 393–396, doi:10.1126/science.245.4916.393.

Howard, A.D., 1994, A detachment-limited model of drainage basin evolution: Water resources research, v. 30, p. 2261–2285, doi:10.1029/94WR00757.

Howard, A.D., 1980, Thresholds in river regimes: Thresholds in geomorphology, p. 227–258.

Hughes Clarke, J.E., 2016, First wide-angle view of channelized turbidity currents links migrating cyclic steps to flow characteristics: Nature communications, v. 7, p. 11896, doi:10.1038/ncomms11896.

Janocko, M., Cartigny, M.B.J., Nemec, W., and Hansen, E.W.M., 2013, Turbidity current hydraulics and sediment deposition in erodible sinuous channels: Laboratory experiments and numerical simulations: Marine and Petroleum Geology, v. 41, p. 222–249, doi:10.1016/j.marpetgeo.2012.08.012.

Johnson, J.P., and Whipple, K.X., 2007, Feedbacks between erosion and sediment transport in experimental bedrock channels: Earth Surface Processes and Landforms, v. 32, p. 1048–1062, doi:10.1002/esp.1471.

Johnson, J.P.L., Whipple, K.X., Sklar, L.S., and Hanks, T.C., 2009, Transport slopes, sediment cover, and bedrock channel incision in the Henry Mountains, Utah: Journal of geophysical research, v. 114, p. W12446, doi:10.1029/2007JF000862.

Kane, I.A., McCaffrey, W.D., and Peakall, J., 2008, Controls on sinuosity evolution within submarine channels: Geology, v. 36, p. 287–290, doi:10.1130/G24588A.1.

Khripounoff, A., Vangriesheim, A., Babonneau, N., Crassous, P., Dennielou, B., and Savoye, B., 2003, Direct observation of intense turbidity current activity in the Zaire submarine valley at 4000 m water depth: Marine geology, v. 194, p. 151–158, doi:10.1016/S0025-3227(02)00677-1.

Leeder, M.R., and Bridges, P.H., 1975, Flow separation in meander bends: Nature, v. 253, p. 338, doi:10.1038/253338a0.

de Leeuw, J., Eggenhuisen, J.T., and Cartigny, M.J.B., 2016, Morphodynamics of submarine channel inception revealed by new experimental approach: Nature communications, v. 7, p. 10886, doi:10.1038/ncomms10886.

Luthi, S. an, 1981, Experiments on non-channelized turbidity currents and their deposits: Marine geology, v. 40, p. M59–M68, doi:10.1016/0025-3227(81)90139-0.

Métivier, F., Lajeunesse, E., and Cacas, M.-C., 2005, Submarine Canyons in the Bathtub: Journal of Sedimentary Research, v. 75, p. 6–11, doi:10.2110/jsr.2005.002.

Middleton, G.V., 1966, Small-scale models of turbidity currents and the criterion for auto-suspension: Journal of Sedimentary Research, v. 36, p. 202–208, doi:10.1306/74D71442-2B21-11D7-8648000102C1865D.

Mitchell, N.C., 2014, Bedrock erosion by sedimentary flows in submarine canyons: Geosphere, v. 10, p. 892–904, doi:10.1130/GES01008.1.

Mohrig, D., and Buttles, J., 2007, Deep turbidity currents in shallow channels: Geology, v. 35, p. 155–158, doi:10.1130/G22716A.1.

Nino, Y., Lopez, F., and Garcia, M., 2003, Threshold for particle entrainment into suspension: Sedimentology, v. 50, p. 247–263, doi:10.1046/j.1365-3091.2003.00551.x.

Nittrouer, J.A., Mohrig, D., and Allison, M., 2011a, Punctuated sand transport in the lowermost Mississippi River: Journal of geophysical research, v. 116, p. F04025, doi:10.1029/2011JF002026.

Nittrouer, J.A., Mohrig, D., Allison, M.A., and Peyret, A.-P.B., 2011b, The lowermost Mississippi River: a mixed bedrock-alluvial channel: Sedimentology, v. 58, p. 1914–1934, doi:10.1111/j.1365-3091.2011.01245.x.

Pirmez, C., Beaubouef, R.T., Friedmann, S.J., and Mohrig, D.C., 2000, Equilibrium profile and baselevel in submarine channels: examples from Late Pleistocene systems and implications for the architecture of deepwater reservoirs, *in* Global deep-water reservoirs: Gulf Coast Section SEPM Foundation 20th Annual Bob F. Perkins Research Conference, p. 782–805.

Rowland, J.C., Hilley, G.E., and Fildani, A., 2010, A Test of Initiation of Submarine Leveed Channels by Deposition Alone: Journal of Sedimentary Research, v. 80, p. 710–727, doi:10.2110/jsr.2010.067.

Shepherd, R.G., and Schumm, S.A., 1974, Experimental Study of River Incision: GSA Bulletin, v. 85, p. 257–268, doi:2.0.CO;2">10.1130/0016-7606(1974)85<257:ESORI>2.0.CO;2.

Shields, A., 1936, Anwendung der Aehnlichkeitsmechanik und der Turbulenzforschung auf die Geschiebebewegung: PhD Thesis Technical University Berlin.

Sklar, L.S., and Dietrich, W.E., 2004, A mechanistic model for river incision into bedrock by saltating bed load: Water resources research, v. 40, doi: 10.1029/2003WR002496.

Smith, J.D., and Hopkins, T.S., 1971, Sediment Transport on the Continental Shelf Off of Washington and Oregon in Light of Recent Current Measurements: Washington Univ., Seattle. Dept. of Oceanography. Atomic Energy Commission, U. S. A.

Straub, K.M., Mohrig, D., Buttles, J., McElroy, B., and Pirmez, C., 2011, Quantifying the influence of channel sinuosity on the depositional mechanics of channelized turbidity currents: A laboratory study: Marine and Petroleum Geology, v. 28, p. 744–760, doi:10.1016/j.marpetgeo.2010.05.014.

Straub, K.M., Mohrig, D., McElroy, B., and Buttles, J., 2008, Interactions between turbidity currents and topography in aggrading sinuous submarine channels: A laboratory study: GSA Bulletin today: a publication of the Geological Society of America, doi: 120/3-4/368/2260.

Symons, W.O., Sumner, E.J., Paull, C.K., Cartigny, M.J.B., Xu, J.P., Maier, K.L., Lorenson, T.D., and Talling, P.J., 2017, A new model for turbidity current behavior based on integration of flow monitoring and precision coring in a submarine canyon: Geology, v. 45, p. 367–370, doi:10.1130/G38764.1.

Vachtman, D., Mitchell, N., and Gawthorpe, R., 2013, Morphologic signatures in submarine canyons and gullies, central USA Atlantic continental margins: v. 41, p. 250–263, doi:10.1016/j.marpetgeo.2012.02.005.

van Rijn Leo C., 1984, Sediment Transport, Part III: Bed forms and Alluvial Roughness: Journal of Hydraulic Engineering, v. 110, p. 1733–1754, doi:10.1061/(ASCE)0733-9429(1984)110:12(1733).

Weill, P., Lajeunesse, E., Devauchelle, O., Métiver, F., Limare, A., Chauveau, B., and Mouazé, D., 2014, Experimental investigation on self-channelized erosive gravity currents: Journal of Sedimentary Research, v. 84, p. 487–498. Doi: 84/6/487/145405.

Whipple, K.X., 2004, Bedrock Rivers and the Geomorphology of Active Orogens: Annual review of earth and planetary sciences, v. 32, p. 151–185, doi:10.1146/annurev.earth.32.101802.120356.

Whipple, K.X., Hancock, G.S., and Anderson, R.S., 2000, River incision into bedrock: Mechanics and relative efficacy of plucking, abrasion, and cavitation: GSA Bulletin, v. 112, p. 490–503, doi:2.0.CO;2">10.1130/0016-7606(2000)112<490:RIIBMA>2.0.CO;2.

Xu, J.P., 2010, Normalized velocity profiles of field-measured turbidity currents: Geology, v. 38, p. 563–566, doi:10.1130/G30582.1.

Xu, J.P., Barry, J.P., and Paull, C.K., 2013, Small-scale turbidity currents in a big submarine canyon: Geology, v. 41, p. 143–146, doi:10.1130/G33727.1.

Xu, J.P., Noble, M.A., and Rosenfeld, L.K., 2004, In-situ measurements of velocity structure within turbidity currents: Geophysical research letters, v. 31, doi:10.1029/2004GL019718.

Yu, B., Cantelli, A., Marr, J., Pirmez, C., O’Byrne, C., and Parker, G., 2006, Experiments on Self-Channelized Subaqueous Fans Emplaced by Turbidity Currents and Dilute Mudflows: Journal of Sedimentary Research, v. 76, p. 889–902, doi:10.2110/jsr.2006.069.

Figures and captions:

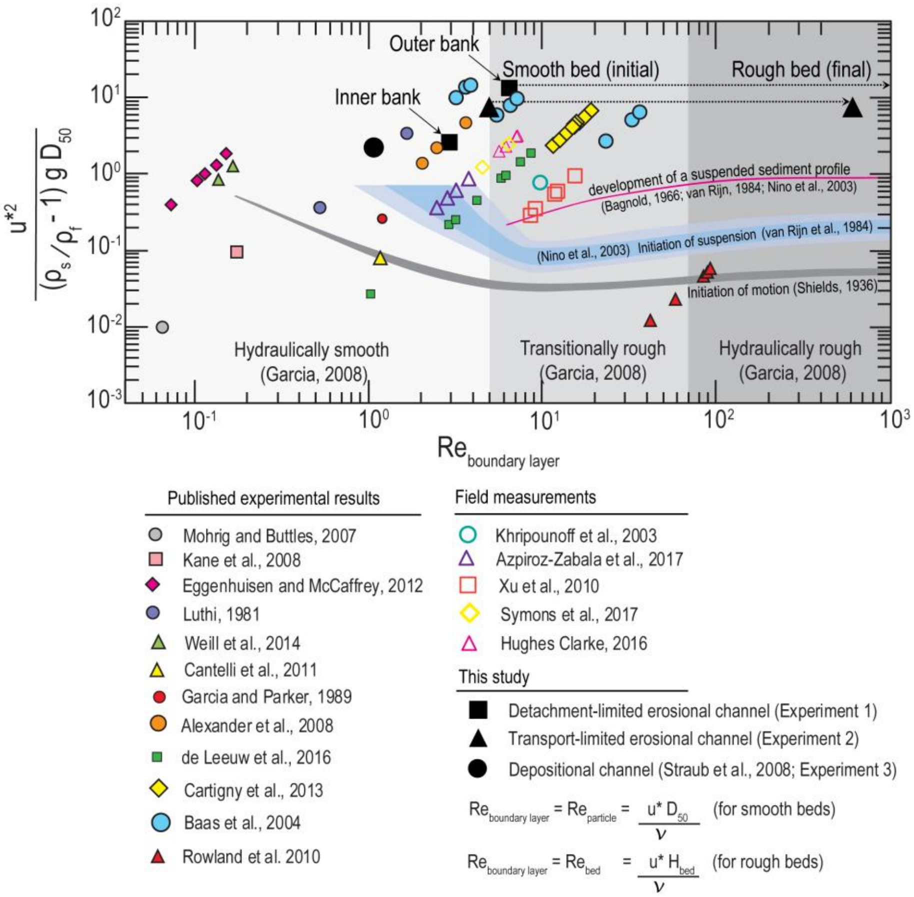

Figure 2: The modified Shield's scaling approach of de Leeuw et al., 2016, used here to compare our experiments to various experimental and field studies. Note that the initial conditions in all 3 experiments presented in this study span the threshold between hydraulically smooth and transitionally rough flow. Bed roughness that evolved in Experiments 1 and 2 increased the turbulence in the boundary, causing it to become hydraulically rough. (Luthi, 1981; Garcia and Parker, 1989; Khripounoff et al., 2003; Baas et al., 2004; Mohrig and Buttles, 2007; Alexander et al., 2007; Straub et al., 2008; Kane et al., 2008; Xu, 2010; Rowland et al., 2010; Cantelli et al., 2011; Eggenhuisen and McCaffrey, 2012; Cartigny et al., 2013; Weill et al., 2014; de Leeuw et al., 2016; Hughes Clarke, 2016; Symons et al., 2017; Azpiroz-Zabala et

al., 2017b). Hydraulic thresholds based on (Shields, 1936; Bagnold, 1966; van Rijn Leo C., 1984; Nino et al., 2003; Garcia, 2008)

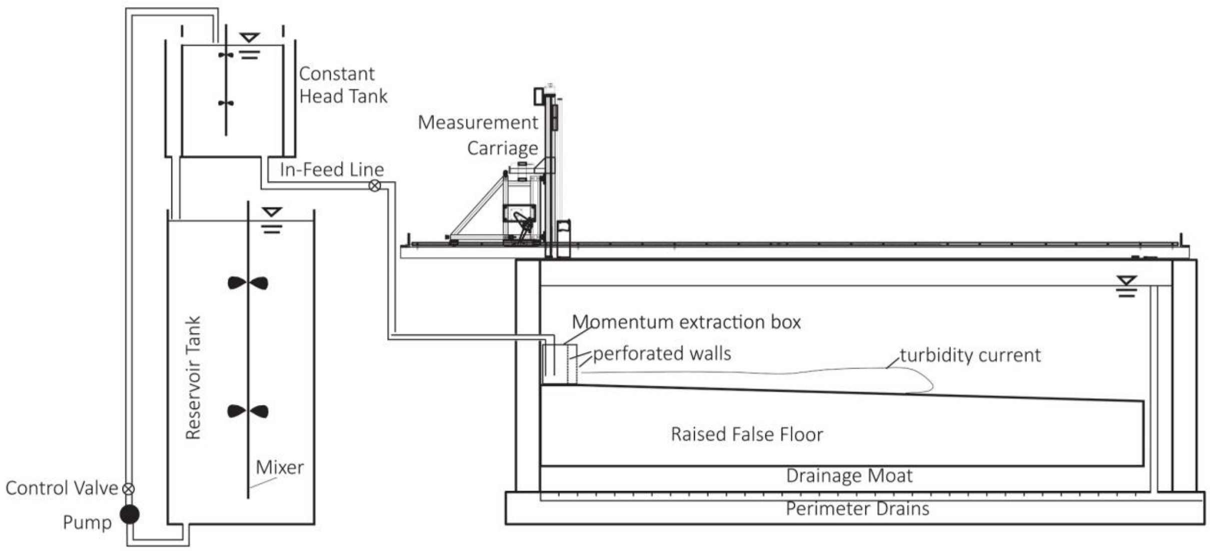

Figure 2: A generalized schematic of the experimental basin set-up used for the three experiments.

441

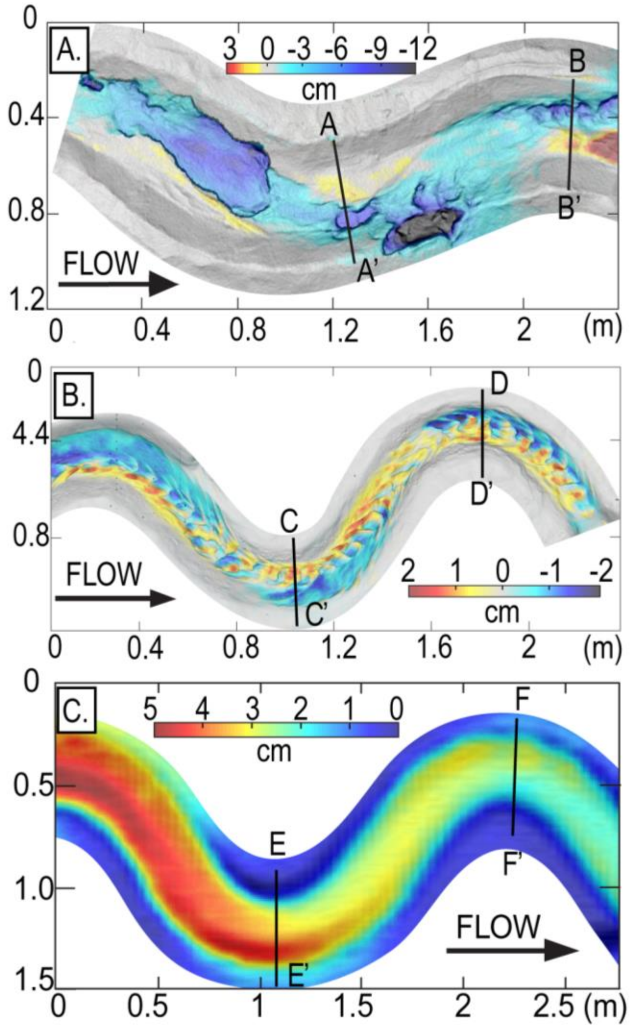

Figure 3: Difference maps defining net elevation change in all three experiments.. (A) Detachment-limited erosion in Experiment 1 resulted in a rough bed patterned with erosional bedforms along a semi-continuous erosional inner channel that followed the path of the high velocity core, and terraces formed at inner banks. (B) Transport-limited erosion in Experiment 2 resulted in a semi-continuous mobile sediment bed, reworked into ripples. (C) Consistent deposition in Experiment 3 resulted in a channel that was persistently aggradational, with the thickest deposits at the outsides of bends.

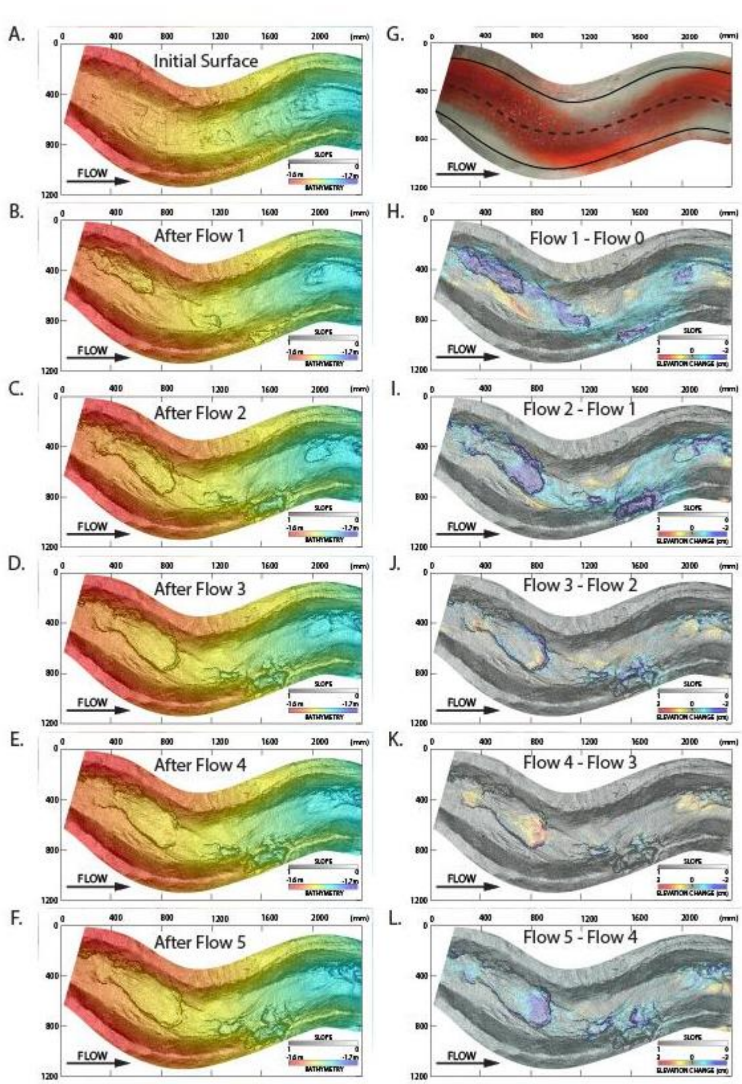

Figure 4: (A-F) Experiment 1 time-lapse laser-scanned topographic maps showing how the 5 experimental currents evolved the experimental channel. (G) Orthorectified overhead photograph showing the pathway of the high velocity core of the current-tracked by red dye with the most intensity. The very small amounts of red dye near the inner banks bear testament to very low velocities in these zones. (H-L) is a series of difference maps that define patterns of erosion and deposition within the experimental channel due to the passage of the 5 density currents. Note how erosion (cold colors) tracks the pathway of the high velocity core (intense red dye in G) and no erosion weak deposition (warm colors) is associated with inner bank zones visited by separated flow (low amount of red dye in G).

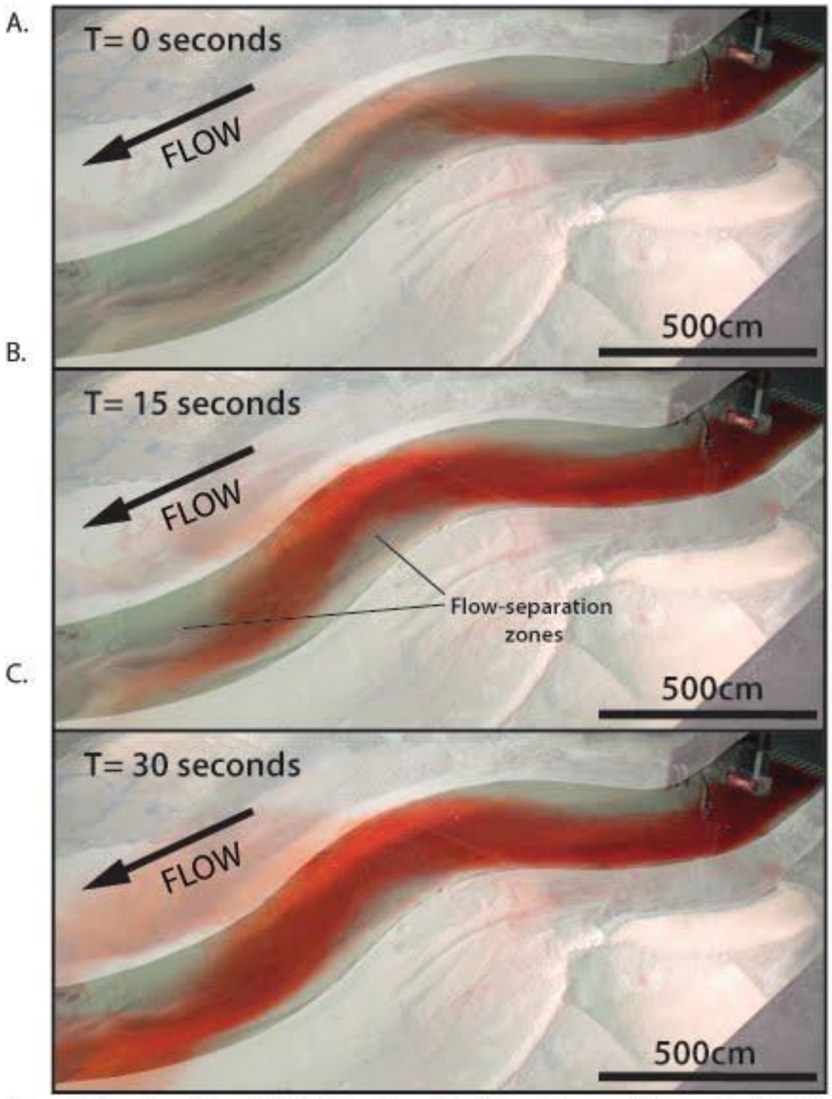

Figure 5: A-C Time lapse photographs showing a pulse of red dye in the current that defines the pathway of the high-velocity core of the current. Low velocity zones where flow separated from the inner banks received the dyed current later than the outside of bends and the dye intensity was always lower than at the outside of bends.

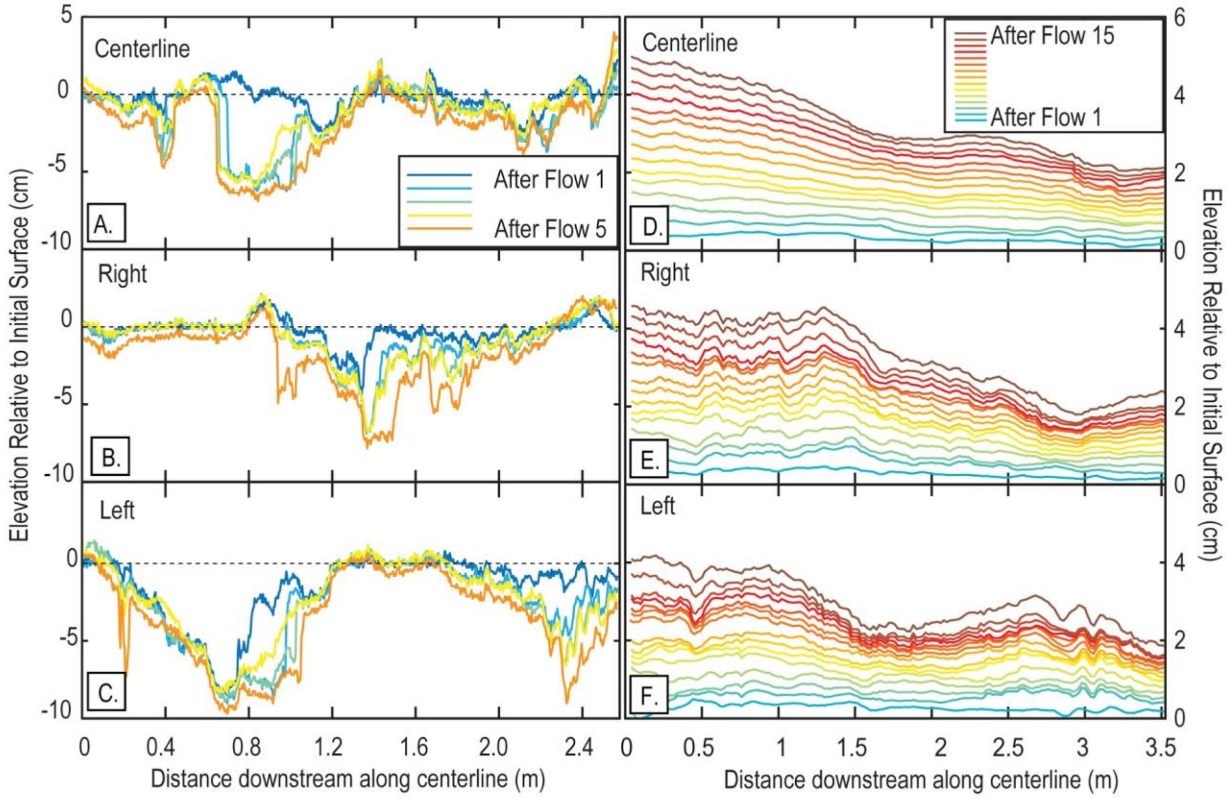

Figure 6: A-C) Change in elevation of the channel bed in Experiment 1 after the passage of 5 consecutive flows, along (A) the centerline, (B) 15 cm right of the centerline, and (C) 15 cm left of the centerline. D-F) Change in elevation of the channel bed in Experiment 3 after the passage of 15 consecutive flows, along (A) the centerline, (B) 5 cm right of the centerline, and (C) 5 cm left of the centerline.

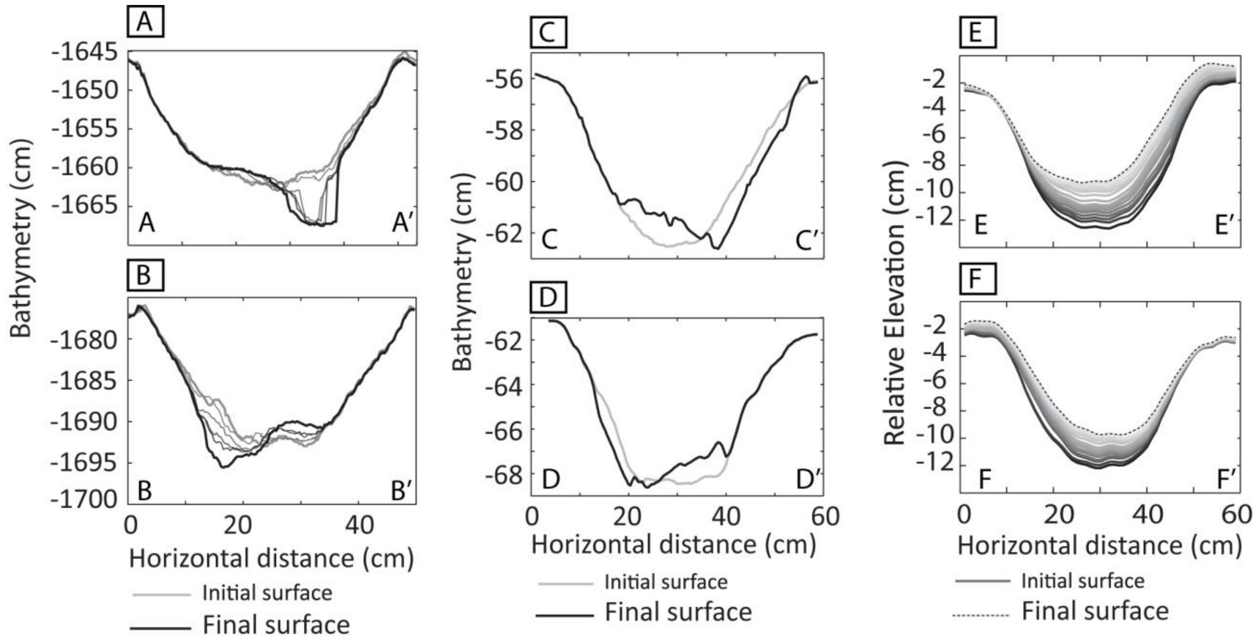

Figure 7: Cross sections showing time-lapse topographic evolution at the apices of the second and third bends in Experiment 1 (A-B), Experiment 2 (C-D) and Experiment 3 (E-F).